Density Evolution Dynamics of Water and Ice

Chang Q Sun,[1,2,*] Xi Zhang,[2] Xiaojian Fu,[3,4] Weitao Zheng,[5]
Jer-lai Kuo,[6] Yichun Zhou,[7] Zexiang Shen,[8] and Ji Zhou[3,†]

[1]*Key Laboratory of Low-Dimensional Materials and Application Technologies, and Faculty of Materials, Optoelectronics and Physics, Xiangtan University, Hunan 411105, China*
[2]*School of Electrical and Electronic Engineering, Nanyang Technological University, Singapore 639798*
[3]*State Key Laboratory of New Ceramics and Fine Processing, Department of Materials Science and Engineering, Tsinghua University, Beijing 100084, China*
[4] *College of Materials Science and Engineering, China Jiliang University, Hangzhou 310018, China*
[5]*School of Materials Science, Jilin University, Changchun 130012, China*
[6]*Institute of Atomic and Molecular Sciences, Academia Sinica, Taipei 10617, Taiwan*
[7]*Key Laboratory of Low-Dimensional Materials and Application Technologies, and Faculty of Materials and Optoelectronics and Physics, Xiangtan University, Hunan 411105, China*
[8]*School of Physics, Nanyang Technological University, Singapore 639798*

(Dated: May 1, 2013)

Coulomb repulsion between the electron pairs of adjacent oxygen (O–O) and the specific-heat difference between the O:H van der Waals bond and the H-O polar-covalent bond determine the angle-length-stiffness relaxation dynamics of the hydrogen bond (O:H-O), which dictates the density and phonon relaxation anomalies of water and ice. The bonding part with relatively lower specific-heat contracts upon cooling, meanwhile, this part forces the other to elongate by different amount via Coulomb repulsion. Both O atoms dislocate in the same direction along the O:H-O with the H atom as the reference origin. In the liquid and solid phases, the softer O:H bond contracts more than the stiffer H-O elongates, hence, an O:H-O cooling contraction and the seemingly "regular" process of cooling densification take place. In the water-ice transition phase, the H-O contracts less than the O:H elongates, leading to an O:H-O elongation and volume expansion during freezing. In ice, the O–O distance is longer than it is in water, resulting in a lower density, so that ice floats.

PACS numbers: 61.20.Ja, 61.30.Hn, 68.08.Bc
Supplementary Information and a molecular dynamics movie are accompanied.

The density anomalies of water and ice and the associated angle-length-stiffness cooling relaxation dynamics of the hydrogen bond (defined as the entire O:H-O) continue to baffle the field, despite the intensive investigations carried out in the past decades [1–16]. Neutron diffraction [11] revealed that both the liquid and the solid H_2O undergoes the seemingly regular process of cooling densification at different rates. At the water-ice transition phase, volume expansion takes place and results in ice with a density 9% lower than the maximal density of water at 277 K [1, 11]. Amazingly, the cooling densification of H_2O is associated with a redshift of the high-frequency H-O phonons ω_H ($\sim$3000 cm^{-1})[18, 19] while the freezing expansion is accompanied with a blueshift of the ω_H [20]. The Raman shift of the low-frequency O:H ($\omega_L \sim 200$ cm^{-1}) phonons in various phases has not yet been systematically characterized. The volume expansion in the freezing temperatures has been well explained using the elegant models such as the mono-phase of tetrahedrally-coordinated structures with thermal fluctuation [4, 6] and the mixed-phase of low- and high- density fragments with thermal modulation of the fragmental ratios [9, 21]. However, little attention has been paid to the mechanism for the seemingly regular process of cooling densification in both the liquid and the solid phase. Therefore, a consistent understanding of the mechanism behind the density and phonon relxation anomalies of water and ice in the full temperature range is greatly desired.

In this Letter, we show that we have been able to reconcile the measured mass-density [1, 11] and Raman-frequency transitions of water/ice based on the framework of O:H-O bond specific-heat disparity, Raman spectroscopy measurements, and molecular dynamics (MD) calculations of the hydrogen bond angle-length-stiffness relaxation of water/ice over the full temperature range. The often overlooked Coulomb repulsion between the electron pairs of the adjacent oxygen (O–O) [22] and the specific-heat disparity of the O:H-O bond are shown to be the key to resolving the density and phonon stiffness puzzles.

We consider the basic structural unit of $O^{\delta-}$:$H^{\delta+}$-$O^{\delta-}$ [22, 23] (also denoted as "O$\cdots$H-O") to represent the $O^{\delta-}$–$O^{\delta-}$ interactions in H_2O, except for H_2O under extremely high pressures and high temperatures [24]. The fraction δ represents the polarity of the $H^{\delta+}$-$O^{\delta-}$ polar-covalent bond. In Fig.1a, the pair of dots on the O in the left represents the nonbonding lone pair ":". The lone pair belongs to the sp^3-orbit hybridized oxygen. The pair of dots on the right represents the bonding electron pair "-". The bonding pair is shared by the H-O polar-covalent bond and centered at sites close to oxygen. The H atom serves as the point of reference in the

O:H-O system. For completeness, we define the entire hydrogen bond to be O:H-O, the intra-molecular polar-covalent bond as the H-O bond and the inter-molecular van der Waals (vdW) bond as the O:H bond hereon.

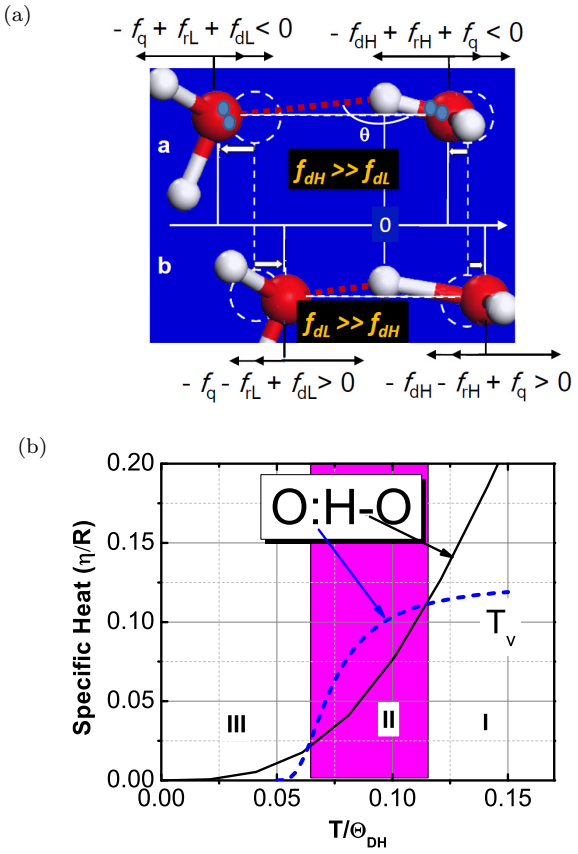

FIG. 1: (a) Forces and relaxation dynamics of the segmented O:H-O bond and (b) the respective specific-heat of the bonding parts. Combined with the Coulomb repulsion f_q between the electron pairs of adjacent O (pairs of dots in a) and the resistance to deformation f_{rx} ($x = H$ for the H-O and L for the O:H segment), the cooling contraction force f_{dx} drives the two parts to relax in the same direction but by different amounts. H atom is the reference origin. (b) Because of the difference in their Debye temperatures (Table I), the specific heat η_L of the O:H rises faster towards the asymptotic maximum value than the η_H. Such a specific-heat decomposition results in three regions that correspond, respectively, to the phases of liquid (I), solid (III), and liquid-solid transition (II) with different specific-heat ratios. R is the gas constant. (The η_L in the solid phase differs from the η_L in the liquid, which does not influence the validity of the hypothesis).

As illustrated in Fig.1a, a hydrogen bond is comprised of the O:H bond (broken lines) and the H-O bond rather than either of them alone [17]. The H-O bond is much shorter, stronger, and stiffer than the O:H bond (comparison shown in Table I). The O:H bond breaks at the evaporating point (T_v) of water (373 K)[18]. However, the H-O bond is much harder to break as the bond energy of ≈4.0 eV [1] is twice that of the C-C bond in diamond (1.84 eV) [25].

The Coulomb repulsion between the electron pairs of adjacent O–O, as represented by the pairs of dots in Fig.1a, is the key to the O:H-O bond relaxation under excitation [1, 22]. Combined with the forces of the Coulomb repulsion, f_q, and resistance to deformation, $f_{rx}(x = H$ for the H-O and L for the O:H bond), the force of cooling contraction, f_{dx} drives these two segments to relax in the same direction but by different amounts.

Generally, the specific heat is regarded as a macroscopic quantity integrated over all bonds, and is the amount of energy required to raise the temperature of the substance by 1 K. However, in dealing with the representative bond of the entire specimen, one has to consider the specific heat per bond that is obtained by dividing the bulk specific heat by the total number of bonds involved. In the case of the O:H-O bond, we need to consider the specific heat (η_x) characteristics of the two segments separately (see Fig.1b) because of the difference in their strengths. The slope of the specific-heat curve is determined by the Debye temperature (Θ_{Dx}) while the integration of the specific-heat curve from 0 K to the melting point T_{mx} [28] is determined by the cohesive energy of the bond E_x. The specific-heat curve of the segment with a relatively lower Θ_{Dx} value will rise to the maximum value faster than the other segment. The Θ_{Dx}, which is lower than the T_{mx}, is proportional to the characteristic frequency of the vibration (ω_x) of the segment. Thus, we have the following relations (see Table I):

$$\begin{cases} \frac{\Theta_{DL}}{\Theta_{DH}} \approx \frac{198}{\Theta_{DH}} \approx \frac{\omega_L}{\omega_H} \approx \frac{200}{3000} \approx \frac{1}{15} \\ \frac{\left(\int_0^{T_{mH}} \eta_H dt\right)}{\left(\int_0^{T_{mL}} \eta_L dt\right)} \approx \frac{E_H}{E_L} \approx \frac{4.0}{0.1} \approx 40 \end{cases} \quad (1)$$

Such a specific-heat disparity between the O:H and the H-O segments creates three temperature regions with different $\frac{\eta_L}{\eta_H}$ ratios, which should correspond to the phases of liquid (I), solid (III), and liquid-solid transition (II).

The consistency in the number of temperature regions (i.e. phases I, II, III) of the proposed specific-heat curve (Fig.1b), the mass-density transition [11], and the O:H-O bond angle-length-stiffness relaxation dynamics (Fig.2 and Fig.3) suggest that the segment with a relatively lower specific heat is thermally more active than the other segment. This thermally active segment serves as the "master" that undergoes cooling contraction while forcing the other "slave" segment to elongate through Coulomb repulsion. Therefore, as can be derived from Fig.1b, the specific-heat ratio, the master segment, and the O–O length change in each temperature region are correlated as follows (see [1] for details):

TABLE I: Summary of the segmental length d_x, strength E_x (energy)[1], Debye temperature Θ_{Dx} [26, 27], stiffness ω_x (vibration frequency), melting point T_{mx}, and the inter-atomic and inter-electron-pair interactions of the O:H-O bond compared with those of the C-C bond in a diamond [25].

Segment (x)	d_x (nm)	E_x (eV)	ω_x (cm^{-1})	Θ_{Dx} (K)	T_{mx} (K)	Interaction
H-O	~0.10	~4.00	>3000	>3000	-	Exchange
O:H	~0.20	~0.05-0.10	~200	198	373	vdW
O–O	-	-	-	-	-	Repulsion
C-C	0.15	1.84	1331	2230	3800	Exchange

$$\left.\begin{array}{ll} \text{II} & (\eta_H < \eta_L):\ f_{dH} > (f_{dL} + f_{rL} + f_{rH}) \\ \text{I, III} & (\eta_L < \eta_H):\ f_{dL} > (f_{dH} + f_{rL} + f_{rH}) \\ \text{Transition} & (\eta_H = \eta_L):\ f_{dH} = f_{dL} \end{array}\right\} \Rightarrow \Delta d_{O-O} \Rightarrow (\Delta V)^{1/3} \left\{\begin{array}{l} < \\ > \\ = \end{array}\right\} 0 \quad (2)$$

Because of the strength difference of the two segments [22], the length of the softer O:H bond always relaxes more than that of the stiffer H-O bond in the same direction: $|\Delta d_L| > |\Delta d_H|$. Thus, we expect the O:H-O bond to relax in the following manners during cooling:
i) In the transition phase II, $\eta_H < \eta_L$ and $f_{dH} \gg f_{dL}$. The H-O bond contraction dominates. The stiffer H-O bond contracts less than the O:H bond elongates, resulting in $\Delta d_{O-O} > 0$. Therefore, a net O–O length gain and an accompanying volume expansion ($\Delta V > 0$) takes place.
ii) In the liquid I and the solid III phase, $\eta_L < \eta_H$ and $f_{dL} \gg f_{dH}$. The master and the slave swap roles. The softer O:H bond contracts significantly more than the H-O bond elongates, $\Delta d_{O-O} < 0$. Hence, a net O–O contraction results in a gain in the mass density.
iii) At the crossing points (Fig.1b), $\eta_H = \eta_L$ and $f_{dH} = f_{dL}$. There is a transition between O–O expansion and contraction, corresponding to the density maximum at 277 K and the density minimum below the freezing point [11, 12].
iv) Meanwhile, the repulsion increases the O:H-O angle θ and polarizes the electron pairs during relaxation.

It has been shown that a segment increases in stiffness as it becomes shorter, while the opposite occurs as it elongates [22, 30]. The Raman shift, which is proportional to the square root of bond stiffness, approximates the length and strength change of the bond during relaxation directly. Approximating the vibration energy of a vibration system to the Taylor series of the inter-atomic potential energy, $u_x(r)$, leads to:

$$\Delta\omega_x \propto \left(\frac{\partial^2 u_x(r)}{\mu \partial r^2}\bigg|_{r=d_x}\right)^{1/2} \propto \frac{\sqrt{E_x/\mu}}{d_x} \propto \sqrt{Y_x d_x} \quad (3)$$

The stiffness is the product of the Young's modulus ($Y_x \propto E_x/d_x^3$) and the length of the segment in question [22]. The μ is the reduced mass of the vibrating dimer. Therefore, the Raman shift measures directly the segmental stiffness.

In order to verify our hypotheses and predictions regarding the O:H-O bond angle-length-stiffness change, the specific-heat disparity, and the density and phonon-frequency anomalies of water/ice, we have conducted Raman measurements and MD calculations as a function of temperature. Two MD computational methods were used in examining the mono- and the mixed-phase models. Details of the experimental and calculation procedures are described in the supplementary information [1].

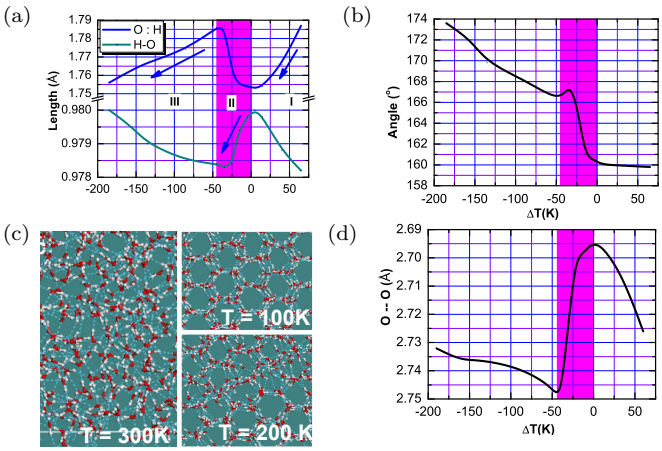

FIG. 2: (a) Segmental length change of the O:H-O bond in the phases of liquid (I), solid (III), and liquid-solid transition (II). Arrows denote the cooling contraction of the master segments, which are coupled with the expansion of the slaves. ΔT = T - T_{max} with T_{max} = 277 K is the maximal density temperature. (b) O:H-O bond angle widening driven by cooling also exhibits three regions. (c) Snapshots of the MD trajectory show that the V-shaped H-O-H molecules remain intact at 300 K because of the robustness of the H-O bond (~4.0 eV/bond) with pronounced quantum fluctuations in the angle and in the d_L in liquid phase. (d) The change of the O–O distance agrees with the measured three-region water and ice densities [1, 11]. In ice, the O–O distance is longer than that in water, which results in ice floating.

Fig.2 shows the MD-derived change of (a) the H-O

bond and the O:H bond length, (b) the O:H-O bond angle θ, (c) the snapshots of the MD trajectory, and (d) the O–O distance as a function of temperature. As shown in Fig.2a, the shortening of the master segments (denoted with arrows) is always coupled with a lengthening of the slaves during cooling. The temperature range of interest consists of three regions: in the liquid region I and the solid region III, the O:H bond contracts significantly more than the H-O bond elongates, resulting in a net loss of the O–O length. Thus, cooling-driven densification of H_2O happens in both the liquid and the solid phase. This mechanism differs completely from the mechanism conventionally adopted for the standard cooling densification of other regular materials in which only one kind of chemical bond is involved. In other materials, cooling shortens and stiffens all the inter-atomic bonds [29]. In contrast, in the transition phase II [11, 13, 14], the master and the slave swap roles. The O:H bond elongates more than the H-O bond shortens so that a net gain in the O–O length occurs.

The θ angle widening (Fig.2b) could also contribute to the volume change. In the liquid phase I, the mean θ valued at 160° remains almost constant. However, the snapshots of the MD trajectory in Fig.2c and the MD movie in the attached [31] show that the V-shaped H-O-H molecules remain intact at 300 K over the entire duration recorded, accompanied by high fluctuations in the θ and the d_L in this regime, which indicates the dominance of tetrahedrally-coordinated water molecules [32]. In region II, cooling widens the θ from 160° to 167°, which contributes a maximum of +1.75% to the O:H-O bond elongation and 5.25% to volume expansion. In phase III, the θ increases from 167° to 174° and this trend results in a maximal value of -2.76% to the volume contraction.

The calculated temperature dependence of the O–O distance as shown in Fig.2d matches satisfactorily with that of the measured density profile [1, 11]. Importantly, the O–O distance is longer in ice than it is in water, and therefore, ice floats.

The measured Raman spectra in Fig.3 show three regions: T>273 K (I), 273 ≥ T ≥ 258 K (II), and T<258 K (III), which are in agreement with the MD calculations [1] and our predictions:

i) At T>273 K (I), abrupt shifts of the ω_L from 75 to 220 cm^{-1} and the ω_H from 3200 to 3150 cm^{-1} indicate ice formation. The coupled ω_L blueshift and ω_H redshift indicate that cooling shortens and stiffens the O:H bond but lengthens and softens the H-O bond in the liquid phase, which confirms the predicted master role of the O:H bond.

ii) At T<258 K (III), the trend of phonon relaxation remains the same as it is in the region of T > 273 K despite a change in the relaxation rates. Cooling from 258 K stiffens the ω_L from 215 to 230 cm^{-1} and softens the ω_H from 3170 to 3100 cm^{-1}. Other supplementary peaks at ∼300 and ∼3400 cm^{-1} are found to be insignificant. The cooling softening of the ω_H mode agrees with that measured using IR spectroscopy [33] of ice clusters of 8∼150 nm sizes. When the temperature drops from 209 to 30 K the ω_H shift from 3253 to 3218 cm^{-1}. For clusters of 5 nm size or smaller, the ω_H shifts by an addition of 40 cm^{-1}.

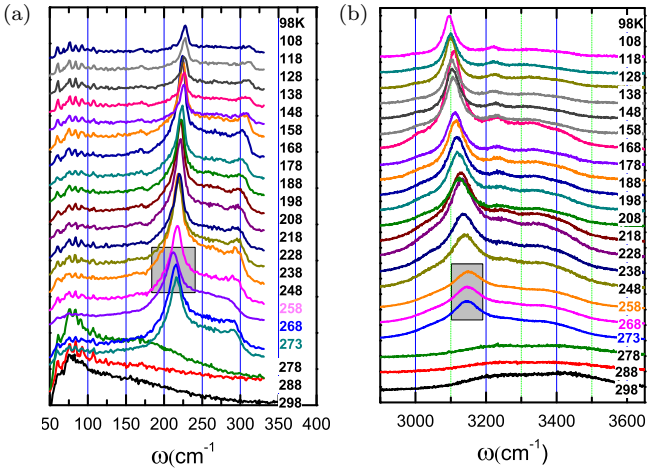

FIG. 3: Temperature dependent Raman shifts of (a) ω_L (the O:H phonon) and (b) ω_H show three regions: T> 273 K (I), 273 K<T<258 K, and T<258 K (III) .

iii) At 273∼258 K (II), the situation reverses. Cooling shifts the ω_H from 3150 to 3170 cm^{-1} and the ω_L from 220 to 215 cm^{-1}, see the shaded areas. Agreeing with the Raman ω_H shift measured in the temperature range between 270 and 273 K [1, 20], the coupling of the ω_H blueshift and the ω_L redshift confirms the exchange in the master and the slave role of the O:H and the H-O bond during freezing.

The MD-movie [31] shows that in the liquid phase, the $H^{\delta+}$ and the $O^{\delta-}$ attract each other between the $H^{\delta+}$:$O^{\delta-}$ but the $O^{\delta-}$-$O^{\delta-}$ repulsion prevents this occurrence. The intact O-H-O motifs are moving restlessly because of the high fluctuations and frequent switching of the $H^{\delta+}$:$O^{\delta-}$ interactions. Furthermore, the coupled cooling ω_L blueshift and ω_H redshift provide further evidence for the persistence of the Coulomb repulsion between the bonding and the nonbonding electron pairs in liquid. The presence of the electron lone pair results from the sp^3-orbit hybridization of oxygen that tends to form tetrahedral bonds with its neighbors [1, 32]. Therefore, the H_2O in the bulk form of liquid could possesses the tetrahedrally-coordinated structures with thermal fluctuation [6, 17, 32]. Snapshots of the MD trajectory in [1] revealed little discrepancy between the mono- and the mixed-phase structural models.

The proposed mechanisms for: i) the seemingly regular processes of cooling densification of the liquid and the solid H_2O, ii) the abnormal freezing expansion, iii) the floating of ice, and, iv) the three-region O:H-O bond angle-length-stiffness relaxation dynamics of water and

ice have been justified. Agreement between our calculations and the measured mass-density [11] and phonon-frequency relaxation dynamics in the temperature range of interest has verified our hypotheses and predictions:
i) Inter-electron-pair Coulomb repulsion and the segmental specific-heat disparity of the O:H-O bond determine the change in its angle, length and stiffness and the density and the phonon-frequency anomalies of water ice.
ii) The segment with a relatively lower specific-heat contracts and drives the O:H-O bond cooling relaxation. The softer O:H bond always relaxes more in length than the stiffer H-O bond does in the same direction. The cooling widening of the O:H-O angle contributes positively to the volume expansion at freezing.
iii) In the liquid and the solid phase, the O:H bond contracts more than the H-O bond elongates, resulting in the cooling densification of water and ice, which is completely different from the process experienced by other regular materials.
iv) In the freezing transition phase, the H-O bond contracts less than the O:H bond lengthens, resulting in expansion during freezing.
v) The O–O distance is larger in ice than it is in water, and therefore, ice floats.
vi) The segment increases in stiffness as it shortens, while the opposite occurs as it elongates. The density variation of water ice is correlated to the incorporative O:H and H-O phonon-frequency relaxation dynamics.

Special thanks to Phillip Ball, Yi Sun, Buddhudu Srinivasa, and John Colligon for their comments and expertise. Financial support received from NSF (Nos.: 21273191, 1033003, and 90922025) China is gratefully acknowledged.

* Electronic address: ecqsun@ntu.edu.sg
† Electronic address: zhouji@Tsinghua.edu.cn

[1] Supplementary Information.
[2] G. N. I. Clark, C. D. Cappa, J. D. Smith, R. J. Saykally, and T. Head-Gordon, Mol. Phys. 108, 1415 (2010).
[3] A. K. Soper, J. Teixeira, and T. Head-Gordon, PNAS 107, E44 (2010).
[4] T. Head-Gordon, and M. E. Johnson, PNAS 103, 7973 (2006).
[5] G. N. Clark, G. L. Hura, J. Teixeira, A. K. Soper, and T. Head-Gordon, PNAS 107, 14003 (2010).
[6] V. Petkov, Y. Ren, and M. Suchomel, J Phys: Condens Matter 24, 155102 (2012).
[7] A. J. Stone, Science 315, 1228 (2007).
[8] K. Stokely, M. G. Mazza, H. E. Stanley, and G. Franzese, PNAS 107, 1301 (2010).
[9] C. Huang, K. T. Wikfeldt, T. Tokushima, D. Nordlund, Y. Harada, U. Bergmann, M. Niebuhr, T. M. Weiss, Y. Horikawa, M. Leetmaa, M. P. Ljungberg, O. Takahashi, A. Lenz, L. Ojame, A. P. Lyubartsev, S. Shin, L. G. M. Pettersson, and A. Nilsson, PNAS 106, 15214 (2009).
[10] N. J. English, and J. S. Tse, Phys. Rev. Lett. 106, 037801 (2011).
[11] F. Mallamace, C. Branca, M. Broccio, C. Corsaro, C. Y. Mou, and S. H. Chen, PNAS 104, 18387 (2007).
[12] F. Mallamace, M. Broccio, C. Corsaro, A. Faraone, D. Majolino, V. Venuti, L. Liu, C. Y. Mou, and S. H. Chen, PNAS 104, 424 (2007).
[13] O. Mishima, and H. E. Stanley, Nature 396, 329 (1998).
[14] E. B. Moore, and V. Molinero, Nature 479, 506 (2011).
[15] V. Molinero, and E. B. Moore, J. Phys. Chem. B 113, 4008 (2009).
[16] C. Wang, H. Lu, Z. Wang, P. Xiu, B. Zhou, G. Zuo, R. Wan, J. Hu, and H. Fang, Phys. Rev. Lett. 103, 137801 (2009).
[17] L. Pauling, Journal of the American Chemical Society 57, 2680 (1935).
[18] P. C. Cross, J. Burnham, and P. A. Leighton, J. Am. Chem. Soc. 59, 1134 (1937).
[19] Y. Yoshimura, S. T. Stewart, H. K. Mao, and R. J. Hemley, J. Chem. Phys. 126, 174505 (2007).
[20] I. Durickovic, R. Claverie, P. Bourson, M. Marchetti, J. M. Chassot, and M. D. Fontana, J. Raman Spec. 42, 1408 (2011).
[21] P. Wernet, D. Nordlund, U. Bergmann, M. Cavalleri, M. Odelius, H. Ogasawara, L. A. Naslund, T. K. Hirsch, L. Ojamae, P. Glatzel, L. G. M. Pettersson, and A. Nilsson, Science 304, 995 (2004).
[22] C. Q. Sun, X. Zhang, and W. T. Zheng, Chem Sci 3, 1455 (2012).
[23] C. Q. Sun, X. Zhang, J. Zhou, Y. L. Huang, Y. Zhou, C., and W. T. Zheng, Phys. Rev. Lett. (LW13133, revised).
[24] Y. Wang, H. Liu, J. Lv, L. Zhu, H. Wang, and Y. Ma, Nat Commun 2, 563 (2011).
[25] C. Kittel, Intrduction to Solid State Physics (John Willey and Sons, New York, 2005).
[26] M. Zhao, W. T. Zheng, J. C. Li, Z. Wen, M. X. Gu, and C. Q. Sun, Phys Rev B 75, 085427 (2007).
[27] M. T. Suter, P. U. Andersson, and J. B. Pettersson, J Chem Phys 125, 174704 (2006).
[28] C. Q. Sun, Prog. Mater Sci. 54, 179 (2009).
[29] C. Q. Sun, L. K. Pan, C. M. Li, and S. Li, Phys Rev B 72, 134301 (2005).
[30] J. W. Li, S. Z. Ma, X. J. Liu, Z. F. Zhou, and C. Q. Sun, Chem. Rev. 112, 2833 (2012).
[31] MD movie showing the quantum fluctuating of the tetrhdral molecules at 300 K.
[32] T. D. Khne, and R. Z. Khaliullin, Nat Commun 4, 1450 (2013).
[33] C. Medcraft, D. McNaughton, C. D. Thompson, D. R. Appadoo, S. Bauerecker, and E. G. Robertson, PCCP 15, 3630 (2013).